

Article

# Synergistic Effect in Zinc Phthalocyanine—Nanoporous Gold Hybrid Materials for Enhanced Photocatalytic Oxidations

David Steinebrunner <sup>1,2</sup> , Günter Schnurpfeil <sup>3</sup>, Andre Wichmann <sup>1</sup>, Dieter Wöhrle <sup>3,\*</sup> and Arne Wittstock <sup>1,2,\*</sup> 

<sup>1</sup> Institute of Applied and Physical Chemistry and Center for Environmental Research and Sustainable Technology, University Bremen, Leobener Str. UFT, 28359 Bremen, Germany; david.steinebrunner@uni-bremen.de (D.S.); awichmann@mail.de (A.W.)

<sup>2</sup> MAPEX Center for Materials and Processes, University Bremen, Bibliothekstr. 1, 28359 Bremen, Germany

<sup>3</sup> Organic and Macromolecular Chemistry, University Bremen, Leobener Str. NW2, 28359 Bremen, Germany; guenter.schnurpfeil@uni-bremen.de

\* Correspondence: woehrle@uni-bremen.de (D.W.); awittstock@uni-bremen.de (A.W.); Tel.: +49-421-21863135 (D.W.); +49-421-21863400 (A.W.)

Received: 23 May 2019; Accepted: 18 June 2019; Published: 20 June 2019



**Abstract:** Nanoporous gold (npAu) supports were prepared as disks and powders by corrosion of Au-Ag alloys. The npAu materials have pore sizes in the range of 40 nm as shown by scanning electron microscopy (SEM). The surface was modified by a self-assembled monolayer (SAM) with an azidohexylthioate and then functionalized by a zinc (II) phthalocyanine (ZnPc) derivative using “click chemistry”. By atomic absorption spectroscopy (AAS) and inductively coupled plasma mass spectrometry (ICP-MS) the content of zinc was determined and the amount of immobilized ZnPc on npAu was calculated. Energy-dispersive X-ray (EDX) spectroscopy gave information about the spatial distribution of the ZnPc throughout the whole porous structure. NpAu and ZnPc are both absorbing light in the visible region, therefore, the heterogeneous hybrid systems were studied as photocatalysts for photooxidations using molecular oxygen. By irradiation of the hybrid system, singlet oxygen is formed, which was quantified using the photooxidation of 1,3-diphenylisobenzofuran (DPBF) as a selective singlet oxygen quencher. The illuminated surface area of the npAu-ZnPc hybrid system and the coverage of the ZnPc were optimized. The synergistic effect between the plasmon resonance of npAu and the photosensitizer ZnPc was shown by selective irradiation and excitation of only the phthalocyanine, the plasmon resonance of the npAu support and both absorption bands simultaneously, resulting in an enhanced photooxidation activity by nearly an order of magnitude.

**Keywords:** photocatalysis; singlet oxygen; nanoporous gold catalyst; zinc phthalocyanine

## 1. Introduction

Plasmonic metal nanostructures exhibit a wide range of properties which are interesting for applications in optical devices, biomedicine and catalysis [1–4]. Their plasmonic properties such as surface plasmon resonance (SPR) and localized surface plasmon resonance (LSPR) depend on the composition, shape and size of the nanostructure [5]. Monolithic nanoporous gold (npAu) as a nanostructured semi-infinite thin film or disk material has recently attracted intense attention due to its unique three-dimensional bicontinuous nanostructures and unique properties such as high catalytic activity, ability as sensor and tuneable plasmonic resonance [6–14]. Such porous nanostructures can be prepared by dealloying of a suitable Au alloy (typically Au-Ag or Au-Cu) using either concentrated nitric acid or electrochemical methods [15–18]. Based on a self-organization process of gold atoms

during the corrosion, an extremely homogeneous porous structure is formed (Figure 1). About 70 per cent of the material is void volume making the material penetrable for gases and liquids. Hence, the specific surface area of this gold sponge, usually in the range of 10–15 m<sup>2</sup>/g, is exposed to the surrounding media [19]. The pore and ligament sizes can be controlled by varying experimental parameters, including the alloy atomic compositions, dealloying time, post synthetic thermal annealing and in case of electrochemical dealloying the employed electrolytes [9]. Nanoporous gold possesses extraordinary optical properties, which are ascribed to the nanoscale infrastructures of hollow channels and metal skeletons in three dimensions [13,14,18]. Localized surface plasmon resonance (LSPR) of npAu can be excited within the wavelength range of visible light with the main absorption at about  $\lambda \sim 520$  nm (Figure 1b) because the unit scale of the metal network is comparable with the mean free path of conduction electrons in the metal ligaments.

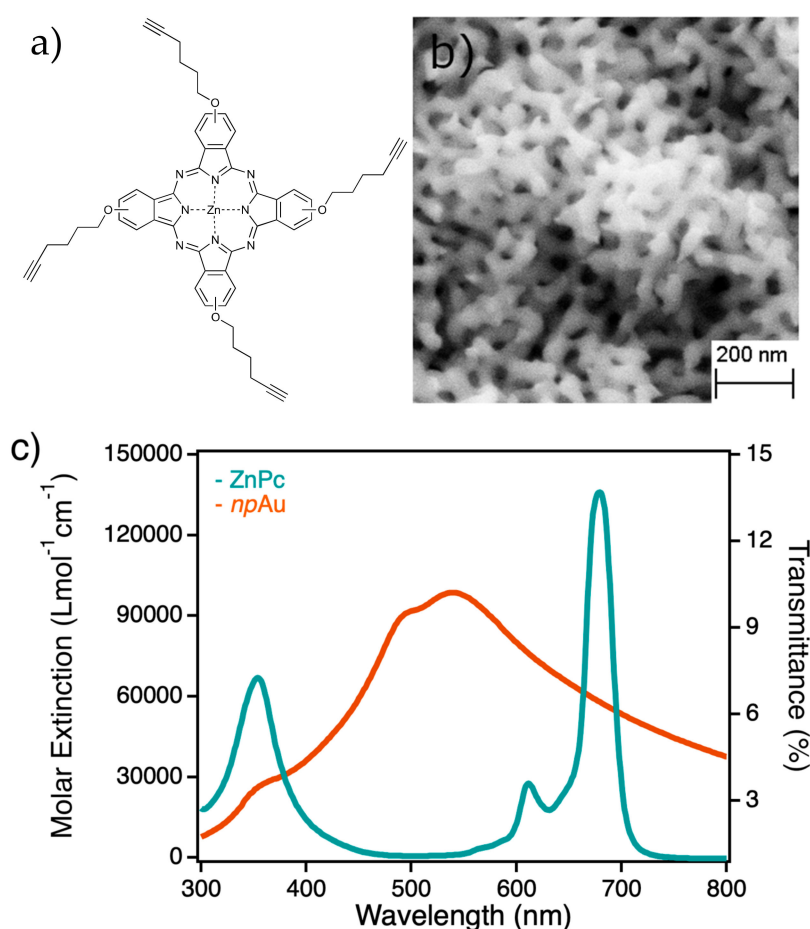


**Figure 1.** Structure of (a) the photosensitizer zinc phthalocyanine 3 used in this study, (b) porous structure of npAu and (c) corresponding optical spectra for zinc (II) phthalocyanine (ZnPc) (cyan) and transmission spectrum of a nanoporous gold foil with a thickness of 100 nm (orange) prepared as described in [20].

The band position at a low wavelength of about  $\lambda \sim 500$  nm does not change when pore sizes reduce from 50 to 10 nm, whereas the band at higher wavelength shifts from  $\lambda \sim 590$  to  $\lambda \sim 545$  nm [13]. In order to enhance the plasmonic properties, a promising strategy is to combine npAu with an additional visible light absorbing chromophore like zinc (II) phthalocyanines and to investigate the photochemical properties of such a hybrid system. Phthalocyanines are absorbing at about  $\lambda \sim 680$  nm with a high extinction coefficient of  $\epsilon_{680} \sim 140,000$  L mol<sup>-1</sup> cm<sup>-1</sup> in dimethylformamide (DMF) (Figure 1c) and are excellent photocatalysts for photooxidations [21,22]. Recently we reported about the binding of a thiol-substituted phthalocyanine zinc (II) complex (ZnPc) by using the principle of

a self-assembled monolayer (SAM) on npAu [23]. We showed in first experiments that the activity in the photooxidation of citronellol in the hybrid system is improved in comparison to the single ZnPc derivative in solution. Based on these previous results, the aim of the present study is to bind a zinc (II) phthalocyanine photosensitizer on different npAu materials in order to investigate and characterize in detail the hybrid material and a possible synergistic effect in the photooxidation reaction. Different npAu systems like disks and powders are prepared and functionalized with a substituted zinc (II) phthalocyanine. Characterizations for all systems include the determination of the immobilized Zn content, the distribution of ZnPc over the whole npAu systems, scanning electron microscopy (SEM) micrographs and penetration depths of visible light in the samples. As reference system for photooxidations, the photooxidation of 1,3-diphenylisobenzofuran (DPBF) is selected because it is a selective and quantitative singlet oxygen quencher that provides clear indications about the activity of the different hybrid systems. Finally, the synergistic effect of the plasmon resonance in npAu systems will be discussed.

## 2. Results

### 2.1. Preparation and Characterization of npAu Functionalized with ZnPc

Free corrosion of the starting alloy in concentrated HNO<sub>3</sub> yielded npAu with a homogeneous porous structure throughout the sample. This method allows a nearly quantitative extraction of the Ag atoms from the starting alloy yielding npAu monoliths with a residual silver concentration below 1 at %, which was confirmed by atomic absorption spectroscopy (AAS) and is in good agreement with previously reported results [24–28]. The pore size of a npAu disk prepared in this way is in the range of 40 nm throughout the sample measured on the surface and along the cross section of the npAu disk (Figures S1 and S2).

The functionalization of the npAu was achieved using a two-step synthetic approach. The npAu material was functionalized in a first step with a SAM consisting of an azide bearing thiolate as linker molecule. The functionalization can be achieved either with the free thiol or the corresponding acetyl protected thiol, which was used in this study [29]. Then the photoactive compound ZnPc 3 was subsequently linked to the functionalized npAu via the azide-alkyne Huisgen cycloaddition, often referred to as click reaction (Figure 2).

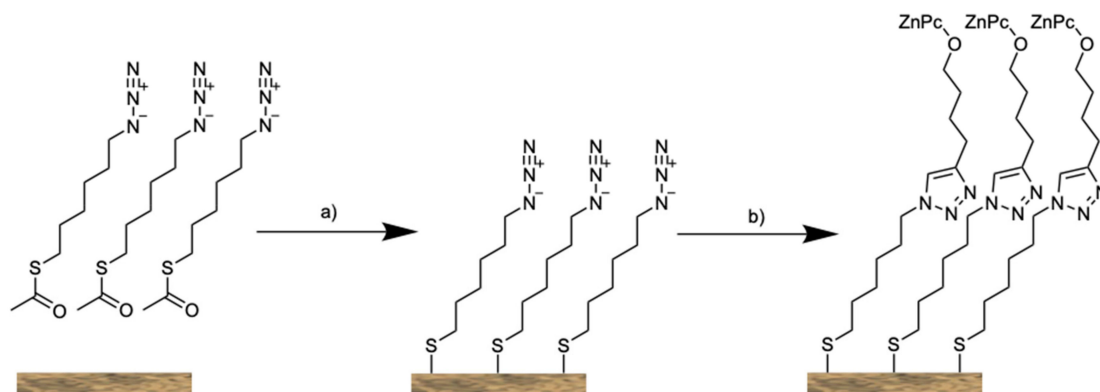


**Figure 2.** Schematic representation of the functionalization of npAu. (a) Formation of a self-assembled monolayer (SAM) using the azide functionalized acetyl protected thiol 1 followed by (b) “click chemistry” to bind the photosensitizer ZnPc 3.

To functionalize such npAu disks by a SAM a mixture of the azidothioate 1 and an unsubstituted spacer, in this case 1-octanethiol, was used. The rationale for using the spacer was to dilute the surface coverage of the sensitizer in order to prevent, for example, steric hindrance and also self-quenching of the excited state of nearby located photosensitizer molecules. The amount of immobilized ZnPc molecules was determined from both, and inductively coupled plasma mass spectrometry (ICP-MS) as

well as AAS after dissolving a fragment of the hybrid system in ultra-pure aqua regia. Both methods showed an immobilized content of ZnPc of  $3 \times 10^{-8}$  mol per functionalized disk. Assuming a typical specific surface area of  $10 \text{ m}^2/\text{g}$  for the npAu, the content of immobilized ZnPc corresponds to  $\sim 0.2\%$  of a monolayer. This value is slightly lower as compared to previous findings in our preliminary work [23]. This can be explained by the fact that in the previous study a linker bearing a  $\text{C}_{11}$  alkyl chain was used whereas in this study we used only a shorter  $\text{C}_6$  linker because a stronger interaction of ZnPc with the npAu surface is expected. The adsorption-desorption equilibrium of SAMs favors the binding of substances with longer chains and therefore results in a lower fraction of the linker molecule in the present study [30]. We further pursued the question of whether the concentration of the ZnPc on the surface can be increased. For this purpose, a second system was prepared without 1-octanethiol as spacer. The synthetic procedure was otherwise the same. ICP-MS and AAS measurements showed, indeed, a higher amount of immobilized ZnPc with  $8 \times 10^{-8}$  mol on the npAu disk, corresponding to an increase in concentration of nearly 300%. The structure of the resulting hybrid photocatalyst was analyzed using SEM, showing that the porous structure of npAu remained in all cases unchanged during the functionalization with the SAM and the ZnPc (Figure 3b).

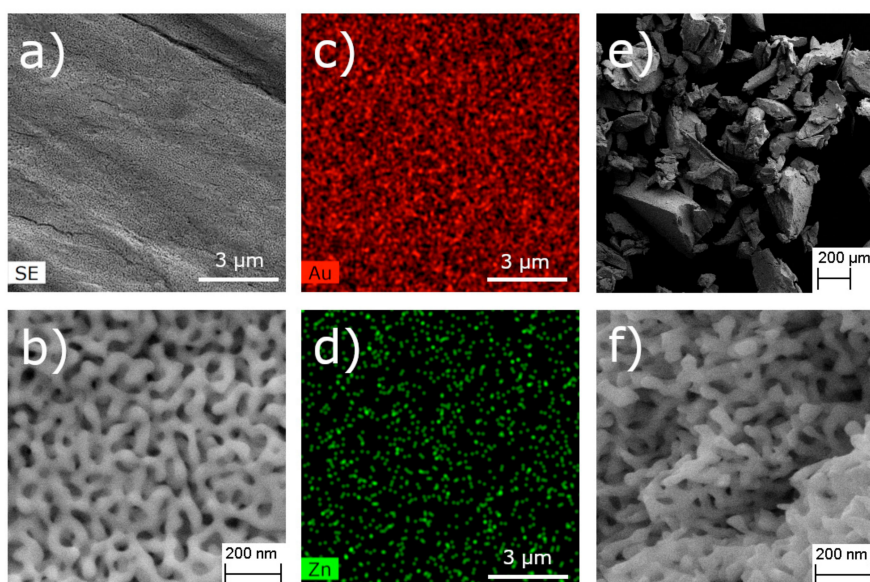


**Figure 3.** Structure of the npAu disk and powder after the two-step functionalization with the azide 1 without spacer and the photosensitizer ZnPc 3 (a) SEM image of the surface used for energy-dispersive X-ray (EDX) measurement, (b) SEM image of the porous structure with a magnification of 100,000, (c) EDX mapping for the element Au and (d) EDX mapping for the element Zn and SEM images of the structure of npAu powder with a magnification of (e) 10,000 and (f) 100,000.

It is now interesting to investigate the distribution of the ZnPc over the whole npAu support. To identify whether the photosensitizer is homogeneously distributed or just forming a multilayer on the outer surface of the monolith, different energy-dispersive X-ray (EDX) measurements were performed. EDX of an npAu disk showed the presence of zinc on the outer surface and, in addition, the EDX mapping showed a homogeneous distribution on the outer surface without the formation of zinc enriched islands (Figure 3c,d). To prove that the ZnPc is not only homogeneously distributed on the outer surface of the npAu disk but also throughout the interior nanoporous structure, a disk was broken in the middle and an EDX linescan was performed along the cross section (Figure S3). It can be seen clearly from the obtained spectrum, that the Zn:Au ratio stays constant over the cross section and therefore the ZnPc is homogeneously distributed throughout the sample. No increase in Zn concentration was found towards the outer surface.

To enhance the irradiated surface area, powders of npAu functionalized with ZnPc 3 were prepared. At first npAu disks were cautiously crushed with metal tweezers. Other methods such as grinding or ball milling had not been successful because the nanoporous structure was destroyed. The result was a heterogeneous powder with particle sizes between 20 and 40  $\mu\text{m}$  as characterized by SEM (Figure S4). The pore size was found to be the same as in the precursor disk (Figure 3f), showing a mean pore size of around 37 nm (Figure S5). Then the npAu powder was modified by a SAM with the azidothioate 1 without spacer and afterwards functionalized with the ZnPc 3 as described for the npAu disks. The quantity of immobilized photosensitizer was the same as on the npAu disk as confirmed by ICP-MS and AAS. EDX linescan measurements over a particle also showed the same homogeneous zinc distribution as it was the case for the cross section of a npAu disk (Figure S6). This is also another proof for the homogenous distribution over the entire surface of the npAu support. Therefore, it can be stated that during the functionalization there is no limitation of the diffusion of the ZnPc 3 (diameter of the Pc ligand without substituent is 1.54 nm and 2.85 nm for the tetrahexyoxo substituted Pc respectively) through the 40 nm pores.

## 2.2. Investigation of Photocatalytic DPBF Oxidations

Irradiation of a npAu disk functionalized with ZnPc in the presence of oxygen leads to singlet oxygen formation which quantitatively reacts with the chemical quencher DPBF. By excitation of ZnPc to the excited triplet state, an energy transfer to triplet oxygen ( $^3\text{O}_2$ ,  $^3\Sigma_g^-$ ) under formation of singlet oxygen ( $^1\text{O}_2$ ,  $^1\Delta_g$ ) occurs with a high quantum yield  $\Phi_\Delta$  of ~0.6 for unsubstituted and alkoxy-substituted ZnPcs [22,31]. DPBF is a chemical quencher for singlet oxygen and reacts selectively and quantitatively via an endoperoxide to 1,2-dibenzoylbenzene (Figure 4a). DPBF is mostly used as standard method for the calculation of singlet oxygen quantum yields obtained by photocatalysts [31–36]. The degradation of DPBF can be followed by the decrease of the absorption at  $\lambda = 415$  nm (Figure S7–S9).

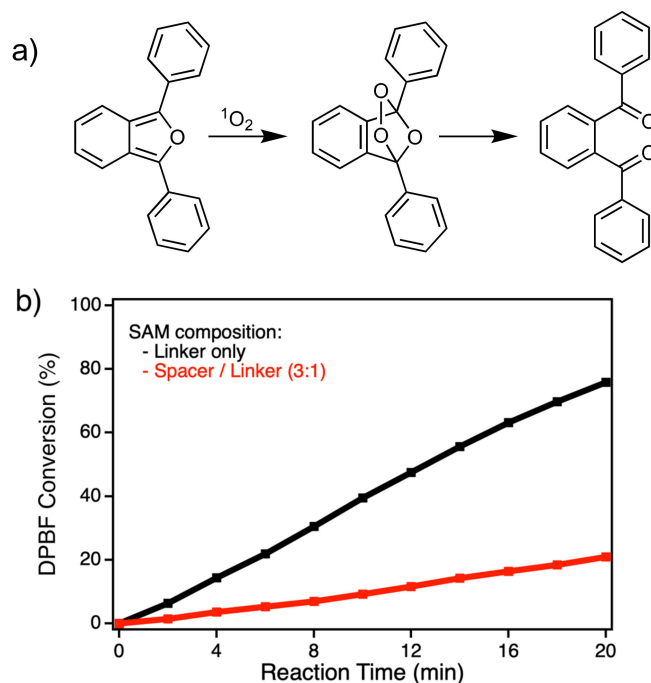


**Figure 4.** (a) Reaction scheme for the photooxidation of 1,3-diphenylisobenzofuran (DPBF) by  $^1\text{O}_2$  via an endoperoxide to 1,2-dibenzoylbenzene; (b) Photocatalytic DPBF conversion comparing the systems with either a 3:1 ratio of linker azidothioate 1: spacer 1-octanethiol (red) and the pure linker hybrid (black).

NpAu disks modified only with an azidothioate 1 SAM exhibit no generation of singlet oxygen in the photooxidation of DPBF 4 under irradiation with a 550 nm cut-on filter. One reason is that the

surface of npAu is protected from interaction with oxygen, as it was already shown by electrochemical methods for SAMs on npAu [23]. However, also unfunctionalized npAu showed no photocatalytic activity under the same irradiation conditions. On the other hand, npAu disks functionalized with ZnPc 3 exhibit a good activity for the photooxidation of DPBF. The question is how many of the ZnPc molecules determined by AAS and ICP-MS are irradiated and thus photochemically active in a modified npAu disk to produce singlet oxygen. As it can be seen in the transmission spectrum of a 100 nm thick npAu foil (Figure 1b), the penetration depth of visible light through the npAu system is only around 10%. However, as shown by the EDX measurements of the npAu disk the photosensitizer is homogeneously distributed throughout the porous structure in the whole sample (Figure S3). Therefore, it is supposed that for a npAu disk with a thickness of 300  $\mu\text{m}$  up to a depth of around 300 nm active parts are excited by illumination. For npAu disks prepared with or without the spacer 1-octanethiol amounts of  $3 \times 10^{-8}$  mol and  $8 \times 10^{-8}$  mol ZnPc molecules were found per npAu disk which corresponds to  $3 \times 10^{-11}$  and  $8 \times 10^{-11}$  mol active parts, respectively.

An increasing degradation of DPBF with higher surface coverage of ZnPc is observed comparing npAu disks with and without the spacer 1-octanethiol (Figure 4b). For a better comparison of the results, the turnover frequency (TOF) values were calculated for both systems from the DPBF conversion determined by UV-Vis spectroscopy (Figure S7a,b) assuming a light penetration depth of 300 nm. TOF values of  $1366.6 \text{ min}^{-1}$  for the disk with and  $2243.9 \text{ min}^{-1}$  without the spacer were found. This result clearly indicates that self-quenching of the excited state of ZnPc on npAu is not an issue in the investigated systems, and the activity only depends on the degree of loading with ZnPc. It is important to mention that no signal of desorbed ZnPc 3 was detected in solution by UV-Vis spectroscopy (Figures S7–S9). This provides evidence for the chemical stability of the photosensitizer on the npAu surface. For comparison, the TOF for the “free” ZnPc photosensitizer in solution was also calculated. In this case, a much lower TOF of  $397.1 \text{ min}^{-1}$  was derived, revealing that the immobilization onto the npAu is increasing the photocatalytic activity by nearly an order of magnitude (Figure S7c).

To point out that the interaction of the surface plasmons of npAu and the ZnPc chromophores is responsible for this enhancement in singlet oxygen production of the hybrid photocatalyst, the photooxidation of DPBF was performed under different irradiation wavelengths (Figure 5). The optical filters were chosen in a way, that selective irradiation of the ZnPc (700 nm), LSPR of npAu (550 nm) as well as irradiation at both wavelengths at the same time was achieved. The photocatalytic DPBF conversion and the calculated TOF values clearly show the synergistic effect of the surface plasmons of npAu (Figure S8). By simultaneous irradiation of both absorption sites, the photocatalytic activity (TOF) is about 40% higher as compared to the irradiation of only the photosensitizer (Figure 5a).

The photocatalytic oxidation of DPBF 4 was also measured by suspending the npAu powder in DMF using the same irradiation wavelengths as described above. The oxidation of DPBF shows the same trends as for the disk but with a higher conversion rate, as expected from the larger illuminated surface area. We measured in this case the highest activity for simultaneous irradiation of the ZnPc and npAu, the conversion was approximately doubled compared to the disks (Figure 5b). This again reflects the synergistic effect between the npAu surface plasmons and the photosensitizer.

For a quantification of the irradiated surface area, the TOF values determined for the npAu hybrid disks were considered, as it is expected that the turnover frequencies are similar for the disk and powder samples. Differences observed in photocatalytic activity achieved by powdering the npAu are due to the enhancement of the illuminated surface area in case of the powders. The results reveal that due to the powdering the illuminated surface area could be enhanced twofold in comparison to the npAu disk (Figure S9). It should be emphasized that the modified npAu powders are still heterogeneous photocatalysts working in the visible region of light. In contrast to gold nanoparticles (AuNPs) which are colloidal dispersed, the npAu powders can be easily recovered by filtration. In view of the fact that gold is an expensive catalyst, this strategy avoids that a large part of the catalytic sites is inactive and does not take part in catalytic turnovers.

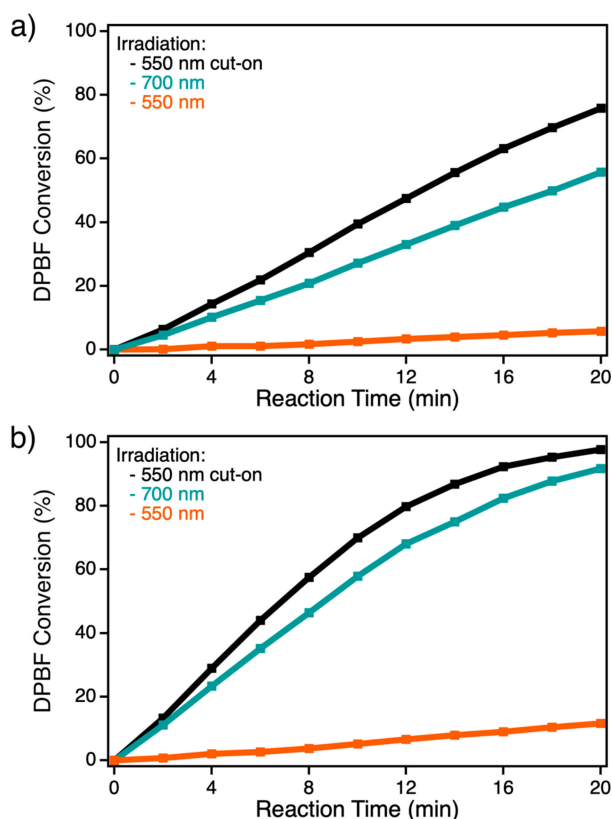


**Figure 5.** Photooxidation of DPBF at different irradiation wavelengths irradiating only the ZnPc absorption using a 700 nm filter (cyan), only the npAu plasmon resonance using a 550 nm filter (orange) or both absorption sites simultaneously using a 550 nm cut-on filter (black) and (a) a ZnPc functionalized npAu disk or (b) a ZnPc functionalized npAu powder as hybrid photocatalyst.

### 3. Discussion

To class our findings, a comparison to results of gold nanoparticles (AuNPs) is evident because they show similar optical properties as npAu. Both systems exhibit a strong surface plasmon resonance in the visible range of the electromagnetic spectrum. Several papers report on zinc(II) phthalocyanines derivatives substituted mainly by thiol-groups and then anchored to AuNPs (sizes of particles ~5 nm) [32,33,37–42]. These conjugates have gained growing interest for drug delivery applications and for photodynamic therapy (PDT) due to the colloidal character of AuNPs [43–45]. Studies in the literature regarding the photophysical properties of these systems report that the fluorescence of ZnPc is strongly quenched [46,47]. Further, an increase of the triplet quantum yields ( $\Phi_T$ ) for a ZnPc derivative on the AuNP conjugate of ~0.80 was observed compared to the same “free” ZnPc in solution with ~0.67 [32]. As a result, the singlet oxygen quantum yield  $\Phi_\Delta$  increased from ~0.6 for unbound ZnPc derivatives in solution to ~0.75 for the same ZnPcs bound to AuNPs [32,33,38–40]. It is assumed that under irradiation with visible light some interaction between AuNP and ZnPc contributes to the formation of singlet oxygen. This observation seems to result from the heavy atoms of AuNP which encourage intersystem crossing to the triplet state of the ZnPc complex through spin orbit coupling [48]. Transferring those results to our system of npAu materials functionalized with ZnPc 3 a higher photocatalytic activity in the photooxidation of DPBF 4 in comparison to the ZnPc in solution was observed under irradiation with light of 700 nm. This direct excitation (Figure 6, red pathway) and the corresponding increase in photocatalytic singlet oxygen production is the result of the mentioned heavy atom effect.

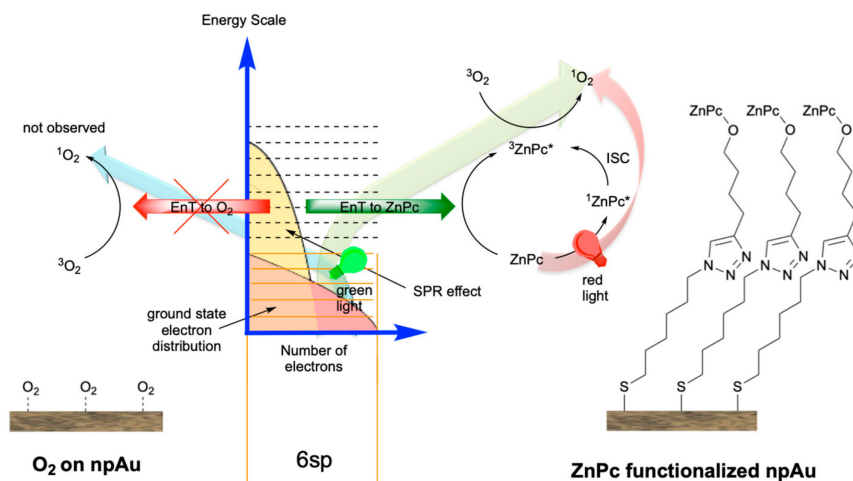


**Figure 6.** Proposed mechanism of  $^1\text{O}_2$  formation in a ZnPc-npAu hybrid system.  $^1\text{O}_2$  generation could be achieved either by direct energy transfer from 550 nm irradiated npAu to adsorbed  $\text{O}_2$  on npAu (blue pathway, not observed in our studies), 550 nm irradiation of npAu followed by energy transfer from npAu to ZnPc (green pathway) or by direct irradiation of ZnPc with 700 nm (red pathway) following the typical mechanism for phthalocyanines via singlet excited state and intersystem crossing (ISC) to the triplet state.

Previous works by the group of Lemmetyinen have also shown charge and energy transfers in such systems, where both an energy transfer from the excited surface plasmons to the photosensitizer and vice versa were observed for a system with a distance of 1 nm between the ZnPc derivative and the AuNP [41,42].

By simultaneous irradiation of both absorption sites in our hybrid system, the photocatalytic activity is significantly higher as compared to the irradiation of only the photosensitizer or only the npAu. It is expected that irradiation of the plasmon resonance of npAu induces an energy transfer (EnT) to the linked photosensitizer, which is then the photocatalytic active site for  $^1\text{O}_2$  formation (Figure 6, green pathway) [49,50]. Similar energy transfers were found in AuNP systems using time resolved spectroscopy techniques and in npAu to nearby located Rhodamine 6G fluorophores [41,42,51]. Electron transfer can be ruled out in our present system as the calculated distance between the surface of npAu and ZnPc is 1.9 nm which is too far for electron transfer with a limit of around 1 nm [52].

It is also known from unfunctionalized AuNPs, which exhibit a major localized surface plasmon resonance at  $\lambda = 520$  nm, that by excitation singlet oxygen can be formed through sensitization of AuNP, but in a low quantum yield of 0.037 [37,53]. It is supposed that oxygen must be adsorbed on the surface due to the short relaxation time of the excited AuNP. The difference in our system is that the surface is blocked by the SAM and therefore no oxygen can adsorb on the surface of npAu. In addition, no photocatalytic activity was found for tests with 550 nm irradiation of unfunctionalized npAu (Figure 6, blue pathway). Only the functionalized npAu-ZnPc system is active under 550 nm irradiation and the energy transfer to the linked photosensitizer is responsible for the observed photocatalytic activity with a TOF of  $161.1 \text{ min}^{-1}$  (Figure S6 and S10c). This supports our proposed mechanism (Figure 6) that a synergistic effect in the form of energy transfer from the npAu to the attached ZnPc is responsible for the observed increase in photocatalytic singlet oxygen formation.

The advantage of npAu compared to AuNPs for catalytic processes is the fact that the colloidal AuNPs have to be considered as pseudo heterogeneous system and behave more as a homogeneous photocatalyst. In contrast, npAu represents a good example for a heterogeneous system that is better suited for heterogeneous photocatalysis, where the noble and expensive metal can be easily recovered by filtration and reused in further catalytic runs, cleaned and functionalized again or reused for the preparation of Au-Ag alloys. Another problem of AuNPs is the lack of stability and agglomeration is often observed. In contrast to AuNPs, npAu exhibit a greater variability with respect to shape and

to apply the catalyst in different forms. In its monolithic form, the shape is completely defined by the shape of the starting alloy, offering the possibility to produce npAu monoliths in form of disks, squares, etc. [54]. They can be easily used in batch as well as flow reactors making them also an interesting material for industrial applications. Its porous structure, i.e., the size of ligaments and pores, which have a direct influence on the localization of the plasmonic resonance, can also be easily adjusted by variation of the dealloying time or a subsequent thermal treatment [13].

## 4. Materials and Methods

### 4.1. Materials

Ag-Au disks with chemical composition of 75:25 at % were prepared within our group according to a previously published procedure [54]. S-(6-azidoethyl)ethanethioate (1) was synthesized starting from 6-bromo-1-hexanol via 6-azidohexan-1-ol and 6-azidoethyl methanesulfonate according to literature procedures (Figure S10) [46,55,56].

4-(Hex-5-yn-oxy)phthalonitrile (2) was synthesized as published previously and 2,9,16,23-Tetrakis (4-hex-5-yn-oxy)phthalocyanine-zinc (II) (3) was obtained as described in the supporting information (Figure S11) [23]. The co-catalyst tris(benzyl-triazolylmethyl)amine (TBTA) was obtained by a modified procedure with a difference in workup as found in the literature [47,57]. 1-Octanethiol (98%) was bought from ABCR, hydroquinone was received from Merck, Cu(MeCN)<sub>4</sub>PF<sub>6</sub> (97%) from Aldrich and 1,3-diphenylisobenzofuran (DPBF (4), > 95%) from TCI. Ethanol (abs., reagent grade), tetrahydrofuran (THF, reagent grade, ≥ 99.0%), DMF (analytical reagent grade, ≥ 99.5%) and HNO<sub>3</sub> (analytical reagent grade, 65 wt %) as well as HNO<sub>3</sub> (NORMATOM, ultra pure for trace analysis, 67 wt %) and HCl (NORMATOM, ultra pure for trace analysis, 34 wt %) were bought at VWR Chemicals (Hannover, Germany) and were used as received without further purification. UV Vis spectra of ZnPc 3, npAu and for the measurements of the photocatalytic oxidations were recorded on a UV-1600PC UV Vis spectrometer from VWR International GmbH (Hannover, Germany). NMR spectra were recorded on a Bruker AVANCE DPX-200 (4.7 Tesla, Bruker, Rheinstetten, Germany) in CDCl<sub>3</sub> unless stated otherwise. IR spectra were recorded on a Nicolet 320 FT-IR spectrometer (Nicolet, Madison, WI, USA) and MS spectra on an Esquire-LC (ESI, direct, Bruker Daltonik GmbH, Bremen, Germany) or MAT95XL (EI, 70 eV, direct, Finnigan MAT, Thermo Fisher Scientific, Waltham, MA, USA) mass spectrometer.

### 4.2. Nanoporous Gold (npAu) Preparation

The preparation of npAu disks was achieved following a general procedure employing a free corrosion technique [25]. Briefly, the alloy disk (Ag: Au 75:25 at %, 5 mm diameter, 300 μm thickness) was placed in concentrated HNO<sub>3</sub> (50 mL, 65 wt %) for 72 h at room temperature. After dealloying, the npAu disk was repeatedly washed with deionized water and dried at ambient atmosphere overnight.

npAu powder was prepared from npAu disks by cautiously fragmentation with metal tweezers. The resulting powder showed a mean particle size of 28 μm as confirmed by scanning electron microscopy.

### 4.3. Hybrid Preparation

The as prepared npAu samples were immersed into an ethanolic solution containing 1 mmol of the SAM precursors (1 (50.3 mg, 0.25 mmol) and 1-octanethiol (109.6 mg, 0.75 mmol) for first system and only 1 (201.2 mg, 1 mmol) for the second system in EtOH (5 mL)) for 72 h. Then the samples were repeatedly washed with EtOH to remove any physisorbed material.

The as prepared functionalized npAu samples with azide groups were immersed into a solution of ZnPc (3, 144.2 μg, 0.15 μmol), Cu(MeCN)<sub>4</sub>PF<sub>6</sub> (931.8 μg, 2.5 μmol), TBTA (1.326 mg, 2.5 μmol) and hydroquinone (272.5 μg, 2.5 μmol) in a THF/H<sub>2</sub>O mixture (5 mL, 3:1 v/v). After a reaction time of 72 h, the sample was repeatedly washed with THF to remove any unbound ZnPc.

#### 4.4. Characterization Methods

The quantity of immobilized ZnPc on npAu was determined by atomic absorption spectroscopy (AAS 5 FL, Jena Analytik AG, Jena, Germany) and inductive coupled-plasma mass spectrometry (ICP-MS, iCAP Q, Thermo Fisher Scientific GmbH, Bremen, Germany) after dissolving 10 mg of the as prepared hybrid sample in ultra pure aqua regia (2 mL) at 60 °C.

For determination of the ligament size of the npAu supports as well as the zinc distribution, the disk was broken in the middle and fixed upright on the microscope sample holder with a conductive carbon tape. Micrographs of the samples' morphology were acquired with a Supra 40 (Zeiss, Oberkochen, Germany) scanning electron microscope operated at 15.0 kV acceleration voltage, 300 pA probe current and 10 mm working distance. The pore sizes were determined by measuring the diameter of at least 250 pores in the obtained SEM images using the program ImageJ. The zinc distribution on the surface and through the porous structure was determined by energy dispersive X-ray spectroscopy (EDX, Bruker XFlash 6/30, Bruker, Berlin, Germany).

#### 4.5. Photocatalytic Oxidation

Photocatalytic oxidations were carried out employing different npAu-ZnPc hybrids as photocatalysts under oxygen atmosphere and irradiation with visible light. As reference reaction for the photocatalytic activity of the hybrid catalysts, the photooxidation of DPBF 4 was chosen. For the measurements a self-built setup consisting of a cylindrical 120 mL stainless steel tube equipped with a condenser, water filter for infrared radiation (IR) cut-off and various optical filters was used (Figure S12). The reaction mixture was stirred using a magnetic stirrer with a constant speed of 600 rpm throughout each catalytic experiment. Irradiation was carried out using a 300 W Xe-arc lamp, with a light intensity of  $180 \text{ mW cm}^{-2}$  after the respective optical filter, which was fixed in every experiment. The whole setup was temperature controlled via a thermostat and held constantly at 25 °C. npAu disks were mounted at the end of the reactor whereas npAu powders were directly added to the reactor. Then the tube was filled with DMF (100 mL) and flushed with O<sub>2</sub> for 10 min. DPBF 4 (1.35 mg, 5 μmol) dissolved in DMF (500 μL) was added, the vessel was closed with a septum and the light source was turned on. The reaction was followed by taking a sample every 120 s via syringe and analysis was carried out by UV Vis spectroscopy. The decrease of DPBF was measured at the absorption maximum of 415 nm ( $\epsilon_{415} = 23,000 \text{ L mol}^{-1} \text{ cm}^{-1}$  in DMF) [31]. The photooxidations followed a zero-order kinetic and were further quantified by the calculation of the respective turnover numbers (TON, mol converted DPBF/mol irradiated ZnPc) and turnover frequencies (TOF, slope of the plot of TON versus reaction time), according to literature for immobilized photosensitizers [58].

### 5. Conclusions

First of all, we point out that our concept of hybrid materials based on nanoporous gold (npAu) and zinc (II) phthalocyanine (ZnPc) was successfully applied for a synergistic and very effective photocatalyst. All samples exhibit a nanoporous structure with an average pore size of 40 nm for npAu disks and powders. It was shown that the ZnPc is homogeneously distributed on the entire surface of the porous npAu materials. The content of immobilized ZnPc was found in the range of  $10^{-8}$  mol per hybrid catalyst and could be considerably enhanced using only the linker molecule to bond the ZnPc. Both components of the hybrid material, npAu ( $\lambda \sim 520 \text{ nm}$ ) and phthalocyanine ( $\lambda \sim 680 \text{ nm}$ ) are absorbing in the visible region of light. The hybrid systems were investigated under oxygen atmosphere and irradiation in the photooxidation of 1,3-diphenylisobenzofurane (DPBF).

We could optimize the hybrid system regarding the surface coverage of npAu with ZnPc giving a system that showed even higher photocatalytic activity than the ZnPc in solution or the npAu. In addition, the synergistic effect between the surface plasmons of npAu and the ZnPc during the photocatalytic oxidation of DPBF was shown by irradiation of the active hybrid system at different wavelengths. The penetration depth of visible light in npAu was investigated and different npAu

supports offering a higher illuminated surface area were studied using powdered npAu. These systems exhibit a significantly higher activity due to the enlarged irradiated surface area. It should be emphasized that a very high excess of DPBF in relation to ZnPc was used (molar ratio DPBF:ZnPc~ $10^5$ :1) showing that we could obtain an extremely active photocatalytic system. Some advantages as heterogeneous catalyst or photocatalyst compared to Au nanoparticles are pointed out. Further studies, which are currently being investigated, will focus on the distance dependence of the energy transfer from npAu to ZnPc by variation of the alkyl chain length between the two components. In addition, npAu functionalized with other photosensitizers such as porphyrins will be studied. In addition, the binding mode of ZnPc to the npAu is still under discussion and further studies are necessary. Subsequently, we will investigate with our hybrid systems the photooxidation of substrates of technical interest.

**Supplementary Materials:** The following are available online at <http://www.mdpi.com/2073-4344/9/6/555/s1>, Figure S1: Representative SEM images of a ZnPc functionalized npAu disk showing the breaking edge with a magnification of (a) 1000; (b) 20,000; (c) 50,000; (d) 100,000. Corresponding pore size distribution shows a Gaussian-distribution and is shown in (e). Figure S2: Representative optical image of a ZnPc functionalized npAu disk with a diameter of 5 mm in (a) and representative SEM images of a npAu disk showing the surface with a magnification of (b) 20,000; (c) 50,000; (d) 100,000. Corresponding pore size distribution shows a Gaussian-distribution and is shown in (e). Figure S3: EDX line scan on the breaking edge of a npAu disk after the two-step functionalization with the azide 1 and the photosensitizer ZnPc 3 showing the ratio of the elements Zn and Au (top) and the corresponding SEM image (bottom) with the position of the line scan (length 333  $\mu\text{m}$ ). Figure S4: Representative SEM images of the npAu powder modified with the linker azidothioate 1 and functionalized with the ZnPc 3 with a magnification of 200 (a) to determine the particle size. Corresponding particle size distribution shows a Gaussian-distribution and is shown in (b). Figure S5: Representative SEM images of the npAu powder modified with the linker azidothioate 1 and functionalized with the ZnPc 3 with a magnification of (a) 60; (b) 20,000; (c) 50,000; (d) 100,000. Corresponding pore size distribution shows a Gaussian-distribution and is shown in (e). Figure S6: EDX line scan on the surface of a npAu powder particle modified with the linker azidothioate 1 and functionalized with the ZnPc 3 showing the ratio of the elements Zn and Au (top) and the corresponding SEM image (bottom) with the position of the line scan. Figure S7: UV Vis spectra for the photooxidation of DPBF over (a) an npAu disk modified with the linker azidothioate 1 and functionalized with the ZnPc 3; (b) a npAu disk with the linker azidothioate 1 in the presence of octanethiol as spacer (1:3) and functionalized with the ZnPc 3. All photooxidations were performed under irradiation with a 550 nm cut-on filter. From the obtained number of converted DPBF, the turnover numbers (TON) were calculated using the illuminated photosensitizer concentration of  $8 \times 10^{-11}$  mol and  $3 \times 10^{-11}$  respectively. (c) For comparison, the photosensitizer 3 in solution with a concentration of  $1 \times 10^{-10}$  was measured. The values of a, b, and c were plotted against the reaction time and the slope obtained by linear regression is the desired turnover frequency (TOF). Figure S8: UV Vis spectra for the photooxidation of DPBF over a npAu disk modified with the linker azidothioate 1 and functionalized with the ZnPc 3 irradiated with (a) 550 nm cut-on filter; (b) 700 nm bandpass filter and (c) 550 nm bandpass filter. From the obtained number of converted DPBF, the turnover numbers (TON) were calculated using the illuminated photosensitizer concentration of  $8 \times 10^{-11}$  mol. The values of a, b, and c were plotted against the reaction time and the slope obtained by linear regression is the desired turnover frequency (TOF). Figure S9: UV Vis spectra for the photooxidation of DPBF over a npAu powder modified with the linker azidothioate 1 and functionalized with the ZnPc 3 irradiated with (a) 550 nm cut-on filter; (b) 700 nm bandpass filter and (c) 550 nm bandpass filter. From the obtained number of converted DPBF and the turnover numbers (TON) from the npAu disks, the illuminated photosensitizer concentration was calculated as  $1.6 \times 10^{-10}$  mol. The values of a, b, and c were plotted against the reaction time and the slope obtained by linear regression is the desired turnover frequency (TOF). Figure S10: Synthesis scheme for the linker S-(6-azidohexyl)ethanethioate 1 starting from 6-bromo-1-hexanol via 6-azidohexan-1-ol and 6-azidohexyl methanesulfonate. Figure S11: Synthesis scheme for the photosensitizer 2,9,16,23-Tetrakis(4-hex-5-yloxy) phthalocyanine-zinc(II) (ZnPc). Figure S12: Schematic representative of the photocatalytic setup modified from [1] with permission from LOT qd GmbH, Darmstadt, Germany. For illumination a scientific light source from LOT qd GmbH equipped with a 300 W Xe arc lamp was used.

**Author Contributions:** Conceptualization, A.W. (Arne Wittstock), D.W. and D.S.; methodology, D.S., G.S. and A.W. (Andre Wichmann); formal analysis, D.S.; investigation, D.S.; resources, A.W. (Arne Wittstock) and D.W.; writing—original draft preparation, D.S.; writing—review and editing, A.W. (Arne Wittstock), D.W. and D.S.; visualization, D.S.; supervision, A.W. (Arne Wittstock) and D.W.; funding acquisition, A.W. (Arne Wittstock) and D.W.

**Funding:** This research was funded by the German Science Foundation (DFG) within the Research Projects WI 4497/3-1 and WO 237/42-1.

**Acknowledgments:** We gratefully acknowledge Petra Witte (Department of Historic Geology and Paleontology, University of Bremen, Bremen, Germany) for experimental support during the SEM and EDX measurements and Cornelia Rybarsch-Steinke (Institute for Applied and Physical Chemistry, University of Bremen, Bremen, Germany) for measuring AAS. We also especially thank Martin Nowak (Institute for Applied and Physical

Chemistry, University of Bremen, Bremen, Germany) for his help during the design of the photocatalysis setup and the fabrication of the reaction vessel. In addition, we thank the lab technician trainees Rebecca Siemering, Jasmin Richter and Rieke Norden for their help within the synthesis part. We gratefully acknowledge reading of the manuscript and discussion with Prof. Marcus Bäumer (Institute for Applied and Physical Chemistry, University of Bremen, Bremen, Germany) and Prof. Anne Staubitz (Institute for Analytical and Organic Chemistry, University of Bremen, Bremen, Germany). We kindly acknowledge the University of Bremen for central payment.

**Conflicts of Interest:** The authors declare no conflict of interest.

## References

1. Krenn, J.R. Watching energy transfer. *Nat. Mater.* **2003**, *2*, 210–211. [[CrossRef](#)] [[PubMed](#)]
2. Pincella, F.; Isozaki, K.; Miki, K. A visible light-driven plasmonic photocatalyst. *Light Sci. Appl.* **2014**, *3*, e133. [[CrossRef](#)]
3. Sotiriou, G.A. Biomedical applications of multifunctional plasmonic nanoparticles. *Wiley Interdiscip. Rev. Nanomed. Nanobiotechnol.* **2013**, *5*, 19–30. [[CrossRef](#)] [[PubMed](#)]
4. Swarnakar, P.; Kanel, S.R.; Nepal, D.; Jiang, Y.; Jia, H.; Kerr, L.; Goltz, M.N.; Levy, J.; Rakovan, J. Silver deposited titanium dioxide thin film for photocatalysis of organic compounds using natural light. *Sol. Energy* **2013**, *88*, 242–249. [[CrossRef](#)]
5. Kelly, K.L.; Coronado, E.; Zhao, L.L.; Schatz, G.C. The Optical Properties of Metal Nanoparticles: The Influence of Size, Shape, and Dielectric Environment. *J. Phys. Chem. B* **2003**, *107*, 668–677. [[CrossRef](#)]
6. Du, X.; Liu, X.; Li, Y.; Wu, C.; Wang, X.; Xu, P. Efficient biocatalyst by encapsulating lipase into nanoporous gold. *Nanoscale Res. Lett.* **2013**, *8*, 180. [[CrossRef](#)]
7. Detsi, E.; Onck, P.; De Hosson, J.T.M. Metallic Muscles at Work: High Rate Actuation in Nanoporous Gold/Polyaniline Composites. *ACS Nano* **2013**, *7*, 4299–4306. [[CrossRef](#)]
8. Wang, K.; Weissmüller, J. Composites of Nanoporous Gold and Polymer. *Adv. Mater.* **2013**, *25*, 1280–1284. [[CrossRef](#)]
9. Wittstock, A.; Biener, J.; Erlebacher, J.; Bäumer, M. *Nanoporous Gold: From an Ancient Technology to a High-Tech Material*; RSC Publishing, RSC Nanoscience and Nanotechnology: London, UK, 2012.
10. Huang, J.-F.; Sun, I.-W. Fabrication and Surface Functionalization of Nanoporous Gold by Electrochemical Alloying/Dealloying of Au–Zn in an Ionic Liquid, and the Self-Assembly of L-Cysteine Monolayers. *Adv. Funct. Mater.* **2005**, *15*, 989–994. [[CrossRef](#)]
11. Okman, O.; Lee, D.; Kysar, J.W. Fabrication of crack-free nanoporous gold blanket thin films by potentiostatic dealloying. *Scr. Mater.* **2010**, *63*, 1005–1008. [[CrossRef](#)]
12. Fujita, T.; Guan, P.; McKenna, K.; Lang, X.; Hirata, A.; Zhang, L.; Tokunaga, T.; Arai, S.; Yamamoto, Y.; Tanaka, N.; et al. Atomic origins of the high catalytic activity of nanoporous gold. *Nat. Mater.* **2012**, *11*, 775. [[CrossRef](#)] [[PubMed](#)]
13. Lang, X.; Quian, L.; Guan, P.; Zi, J.; Chen, M. Localized surface plasmon resonance of nanoporous gold. *Appl. Phys. Lett.* **2011**, *98*, 093701. [[CrossRef](#)]
14. Zhao, F.; Zeng, J.; Shih, W.-C. Nanoporous Gold Nanocomposites as a Versatile Platform for Plasmonic Engineering and Sensing. *Sensors* **2017**, *17*, 1519. [[CrossRef](#)] [[PubMed](#)]
15. Erlebacher, J.; Aziz, M.J.; Karma, A.; Dimitrov, N.; Sieradzki, K. Evolution of nanoporosity in dealloying. *Nature* **2001**, *410*, 450. [[CrossRef](#)] [[PubMed](#)]
16. Dixon, M.C.; Daniel, T.A.; Hieda, M.; Smilgies, D.M.; Chan, M.H.W.; Allara, D.L. Preparation, Structure, and Optical Properties of Nanoporous Gold Thin Films. *Langmuir* **2007**, *23*, 2414–2422. [[CrossRef](#)] [[PubMed](#)]
17. Zeng, J.; Zhao, F.; Li, M.; Li, C.-H.; Lee, T.R.; Shih, W.-C. Morphological control and plasmonic tuning of nanoporous gold disks by surface modifications. *J. Mater. Chem. C* **2015**, *3*, 247–252. [[CrossRef](#)]
18. Detsi, E.; Salverda, M.; Onck, P.R.; De Hosson, J.T.M. On the localized surface plasmon resonance modes in nanoporous gold films. *J. Appl. Phys.* **2014**, *115*, 044308. [[CrossRef](#)]
19. Cattarin, S.; Kramer, D.; Lui, A.; Musiani, M.M. Preparation and Characterization of Gold Nanostructures of Controlled Dimension by Electrochemical Techniques. *J. Phys. Chem. C* **2007**, *111*, 12643–12649. [[CrossRef](#)]
20. Ding, Y.; Kim, Y.-J.; Erlebacher, J. Nanoporous Gold Leaf: “Ancient Technology”/Advanced Material. *Adv. Mater.* **2004**, *16*, 1897–1900. [[CrossRef](#)]

21. Wöhrle, D.; Suvorova, O.; Gerdes, R.; Bartels, O.; Lapok, L.; Baziakina, N.; Makarov, S.; Slodek, A. Efficient oxidations and photooxidations with molecular oxygen using metal phthalocyanines as catalysts and photocatalysts. *J. Porphyrins Phthalocyanines* **2004**, *08*, 1020–1041. [[CrossRef](#)]
22. Shinohara, H.; Tsaryova, O.; Schnurpfeil, G.; Wöhrle, D. Differently substituted phthalocyanines: Comparison of calculated energy levels, singlet oxygen quantum yields, photo-oxidative stabilities, photocatalytic and catalytic activities. *J. Photochem. Photobiol. A Chem.* **2006**, *184*, 50–57. [[CrossRef](#)]
23. Wichmann, A.; Schnurpfeil, G.; Backenköhler, J.; Kolke, L.; Azov, V.A.; Wöhrle, D.; Bäumer, M.; Wittstock, A. A versatile synthetic strategy for nanoporous gold–organic hybrid materials for electrochemistry and photocatalysis. *Tetrahedron* **2014**, *70*, 6127–6133. [[CrossRef](#)]
24. Wittstock, A.; Wichmann, A.; Biener, J.; Bäumer, M. Nanoporous gold: A new gold catalyst with tunable properties. *Faraday Discuss.* **2011**, *152*, 87–98. [[CrossRef](#)] [[PubMed](#)]
25. Lackmann, A.; Bäumer, M.; Wittstock, G.; Wittstock, A. Independent control over residual silver content of nanoporous gold by galvanodynamically controlled dealloying. *Nanoscale* **2018**, *10*, 17166–17173. [[CrossRef](#)] [[PubMed](#)]
26. Forty, A.J.; Durkin, P. A micromorphological study of the dissolution of silver-gold alloys in nitric acid. *Philos. Mag. A* **1980**, *42*, 295–318. [[CrossRef](#)]
27. Martínez, L.L.; Segarra, M.; Fernández, M.; Espiell, F. Kinetics of the dissolution of pure silver and silver-gold alloys in nitric acid solution. *Metall. Trans. B* **1993**, *24*, 827–837. [[CrossRef](#)]
28. Qian, L.H.; Chen, M.W. Ultrafine nanoporous gold by low-temperature dealloying and kinetics of nanopore formation. *Appl. Phys. Lett.* **2007**, *91*, 083105. [[CrossRef](#)]
29. Tour, J.M.; Jones, L.; Pearson, D.L.; Lamba, J.J.S.; Burgin, T.P.; Whitesides, G.M.; Allara, D.L.; Parikh, A.N.; Atre, S. Self-Assembled Monolayers and Multilayers of Conjugated Thiols,  $\alpha,\omega$ -Dithiols, and Thioacetyl-Containing Adsorbates. Understanding Attachments between Potential Molecular Wires and Gold Surfaces. *J. Am. Chem. Soc.* **1995**, *117*, 9529–9534. [[CrossRef](#)]
30. Bain, C.D.; Whitesides, G.M. Formation of monolayers by the coadsorption of thiols on gold: Variation in the length of the alkyl chain. *J. Am. Chem. Soc.* **1989**, *111*, 7164–7175. [[CrossRef](#)]
31. Spiller, W.; Kliesch, H.; Wöhrle, D.; Hackbarth, S.; Röder, B.; Schnurpfeil, G. Singlet oxygen quantum yields of different photosensitizers in polar solvents and micellar solutions. *J. Porphyrins Phthalocyanines* **1999**, *2*, 145–158. [[CrossRef](#)]
32. Moeno, S.; Antunes, E.; Nyokong, T. Synthesis and photophysical properties of a novel zinc photosensitizer and its gold nanoparticle conjugate. *J. Photochem. Photobiol. A* **2011**, *222*, 343–350. [[CrossRef](#)]
33. Masilela, N.; Antunes, E.; Nyokong, T. Axial coordination of zinc and silicon phthalocyanines to silver and gold nanoparticles: an investigation of their photophysicochemical and antimicrobial behavior. *J. Porphyrins Phthalocyanines* **2013**, *17*, 417–430. [[CrossRef](#)]
34. Karimi, A.R.; Khodadadi, A.; Hadizadeh, M. A nanoporous photosensitizing hydrogel based on chitosan cross-linked by zinc phthalocyanine: an injectable and pH-stimuli responsive system for effective cancer therapy. *RSC Adv.* **2016**, *6*, 91445–91452. [[CrossRef](#)]
35. Maree, M.D.; Kuznetsova, N.; Nyokong, T. Silicon octaphenoxypthalocyanines: photostability and singlet oxygen quantum yields. *J. Photochem. Photobiol. A* **2001**, *140*, 117–125. [[CrossRef](#)]
36. Erdoğmuş, A.; Nyokong, T. Novel, soluble, FluXoro functional substituted zinc phthalocyanines; synthesis, characterization and photophysicochemical properties. *Dyes Pigm.* **2010**, *86*, 174–181. [[CrossRef](#)]
37. Pasparakis, G. Light-Induced Generation of Singlet Oxygen by Naked Gold Nanoparticles and its Implications to Cancer Cell Phototherapy. *Small* **2013**, *9*, 4130–4134. [[CrossRef](#)] [[PubMed](#)]
38. Hone, D.C.; Walker, P.I.; Evans-Gowing, R.; FitzGerald, S.; Beeby, A.; Chambrier, I.; Cook, M.J.; Russell, D.A. Generation of Cytotoxic Singlet Oxygen via Phthalocyanine-Stabilized Gold Nanoparticles: A Potential Delivery Vehicle for Photodynamic Therapy. *Langmuir* **2002**, *18*, 2985–2987. [[CrossRef](#)]
39. Nombona, N.; Antunes, E.; Litwinski, C.; Nyokong, T. Synthesis and photophysical studies of phthalocyanine–gold nanoparticle conjugates. *Dalton Trans.* **2011**, *40*, 11876–11884. [[CrossRef](#)]
40. García Calavia, P.; Marín, M.J.; Chambrier, I.; Cook, M.J.; Russell, D.A. Towards optimisation of surface enhanced photodynamic therapy of breast cancer cells using gold nanoparticle–photosensitiser conjugates. *Photochem. Photobiol. Sci.* **2018**, *17*, 281–289. [[CrossRef](#)]

41. Kotiaho, A.; Lahtinen, R.; Efimov, A.; Metsberg, H.-K.; Sariola, E.; Lehtivuori, H.; Tkachenko, N.V.; Lemmetyinen, H. Photoinduced Charge and Energy Transfer in Phthalocyanine-Functionalized Gold Nanoparticles. *J. Phys. Chem. C* **2010**, *114*, 162–168. [[CrossRef](#)]
42. Kotiaho, A.; Lahtinen, R.; Lemmetyinen, H. Photoinduced processes in chromophore–gold nanoparticle assemblies. *Pure Appl. Chem.* **2011**, *83*, 813. [[CrossRef](#)]
43. Usuda, J.; Chiu, S.-m.; Murphy, E.S.; Lam, M.; Nieminen, A.-L.; Oleinick, N.L. Domain-dependent Photodamage to Bcl-2: A membrane anchorage region is needed to form the target of phthalocyanine photosensitization. *J. Biol. Chem.* **2003**, *278*, 2021–2029. [[CrossRef](#)] [[PubMed](#)]
44. Choi, S.-E.; Sohn, S.; Cho, J.-W.; Shin, E.-A.; Song, P.-S.; Kang, Y. 9-Hydroxypheophorbide  $\alpha$ -induced apoptotic death of MCF-7 breast cancer cells is mediated by c-Jun N-terminal kinase activation. *J. Photochem. Photobiol. C* **2004**, *73*, 101–107. [[CrossRef](#)]
45. Haywood-Small, S.L.; Vernon, D.I.; Griffiths, J.; Schofield, J.; Brown, S.B. Phthalocyanine-mediated photodynamic therapy induces cell death and a G0/G1 cell cycle arrest in cervical cancer cells. *Biochem. Biophys. Res. Commun.* **2006**, *339*, 569–576. [[CrossRef](#)] [[PubMed](#)]
46. Chang, S.-M.; Tu, Z.; Jan, H.-M.; Pan, J.-F.; Lin, C.-H. Rapid synthesis of oligomannosides with orthogonally protected monosaccharides. *Chem. Commun.* **2013**, *49*, 4265–4267. [[CrossRef](#)] [[PubMed](#)]
47. Brassard, C.J.; Zhang, X.; Brewer, C.R.; Liu, P.; Clark, R.J.; Zhu, L. Cu(II)-Catalyzed Oxidative Formation of 5,5'-Bistriazoles. *J. Org. Chem.* **2016**, *81*, 12091–12105. [[CrossRef](#)] [[PubMed](#)]
48. Koziar, J.C.; Cowan, D.O. Photochemical heavy-atom effects. *Acc. Chem. Res.* **1978**, *11*, 334–341. [[CrossRef](#)]
49. Zhu, H.; Chen, X.; Zheng, Z.; Ke, X.; Jaatinen, E.; Zhao, J.; Guo, C.; Xie, T.; Wang, D. Mechanism of supported gold nanoparticles as photocatalysts under ultraviolet and visible light irradiation. *Chem. Commun.* **2009**, 7524–7526. [[CrossRef](#)] [[PubMed](#)]
50. Sarina, S.; Waclawik, E.R.; Zhu, H. Photocatalysis on supported gold and silver nanoparticles under ultraviolet and visible light irradiation. *Green Chem.* **2013**, *15*, 1814–1833. [[CrossRef](#)]
51. Chen, C.; Zhang, L.; Yang, M.; Tao, C.; Han, Z.; Chen, B.; Zeng, H. Size and distance dependent fluorescence enhancement of nanoporous gold. *Opt. Express* **2017**, *25*, 9901–9910. [[CrossRef](#)]
52. Trammell, S.A.; Griva, I.; Spano, A.; Tsoi, S.; Tender, L.M.; Schnur, J.; Lebedev, N. Effects of Distance and Driving Force on Photoinduced Electron Transfer between Photosynthetic Reaction Centers and Gold Electrodes. *J. Phys. Chem. C* **2007**, *111*, 17122–17130. [[CrossRef](#)]
53. Vankayala, R.; Sagadevan, A.; Vijayaraghavan, P.; Kuo, C.-L.; Hwang, K.C. Metal Nanoparticles Sensitize the Formation of Singlet Oxygen. *Angew. Chem. Int. Ed.* **2011**, *50*, 10640–10644. [[CrossRef](#)] [[PubMed](#)]
54. Wittstock, A.; Wichmann, A.; Bäumer, M. Nanoporous Gold as a Platform for a Building Block Catalyst. *ACS Catal.* **2012**, *2*, 2199–2215. [[CrossRef](#)]
55. Sodji, Q.H.; Patil, V.; Kornacki, J.R.; Mrksich, M.; Oyelere, A.K. Synthesis and Structure–Activity Relationship of 3-Hydroxypyridine-2-thione-Based Histone Deacetylase Inhibitors. *J. Med. Chem.* **2013**, *56*, 9969–9981. [[CrossRef](#)] [[PubMed](#)]
56. Ligeour, C.; Meyer, A.; Vasseur, J.-J.; Morvan, F. Bis- and Tris-Alkyne Phosphoramidites for Multiple 5'-Labeling of Oligonucleotides by Click Chemistry. *Eur. J. Org. Chem.* **2012**, *2012*, 1851–1856. [[CrossRef](#)]
57. Chan, T.R.; Hilgraf, R.; Sharpless, K.B.; Fokin, V.V. Polytriazoles as Copper(I)-Stabilizing Ligands in Catalysis. *Org. Lett.* **2004**, *6*, 2853–2855. [[CrossRef](#)] [[PubMed](#)]
58. Han, X.; Bourne, R.A.; Poliakkoff, M.; George, M.W. Immobilised photosensitisers for continuous flow reactions of singlet oxygen in supercritical carbon dioxide. *Chem. Sci.* **2011**, *2*, 1059–1067. [[CrossRef](#)]

